Gas–Liquid Mass Transfer to Single Bubbles: Effect of Surface Contamination

Jorge M. T. Vasconcelos, Sandra P. Orvalho, and Sebastião S. Alves
Centro de Eng. Biológica e Química, Dept. of Chemical Engineering, Instituto Superior Técnico, 1049-001 Lisboa, Portugal

The dissolution of single bubbles of gases of low solubility kept stationary in a downward stream of water was studied. In "clean" water, two regimes are identified. Initially, the process is fast, consistent with the theory for circulating bubbles. Then, the mass-transfer rate falls sharply to that predicted for solid spheres. Transition times and transition diameters vary widely with experimental conditions. In untreated water, only the second regime is found. Results are explained in terms of the kinetics of trace surfactant accumulation at the interface. An adaptation of the stagnant-cap model is proposed, with surface immobilization expressed in terms of interface dynamics. The model yields good prediction of the transition point for a very large set of conditions, including different gases at various concentrations in the liquid stream and a wide range of initial bubble diameters.

Introduction

Dispersion of gas bubbles in liquids is the basis of many mass-transfer operations in chemical engineering practice. One of the most important parameters for the design of mass-transfer apparatus and the economy of the processes is the liquid-side mass-transfer coefficient, k_L, or, under dimensionless form, the Sherwood number, $Sh = k_L d_e/D$.

The mass-transfer coefficient of dissolving bubbles is known to depend upon interface mobility (Griffith, 1960). If the interface is mobile, the contact time with the liquid is short, the penetration of the dissolved gas is slight, and Higbie's theory is valid (Bird et al., 1960). This leads to the same result as Boussinesq's solution for fluid spheres in potential flow (Griffith 1960) or the boundary-layer analysis around the rapidly moving interface at very high *Re* (Lochiel and Calderbank, 1964)

$$Sh = 1.13 Re^{1/2} Sc^{1/2} \tag{1}$$

where *Re* is the Reynolds number and *Sc* the Schmidt number.

If the bubble surface is rigid, the mass-transfer coefficient approaches the values predicted by laminar boundary-layer theory, following the equation proposed by Froessling for solid spheres (Calderbank, 1959)

$$Sh = cRe^{1/2} Sc^{1/3} \tag{2}$$

with constant $c \sim 0.6$, experimental values having been found between 0.42 and 0.95 (Lochiel and Calderbank, 1964).

The question of whether a bubble has a mobile or an immobile surface, or something in between, has since long been related to the presence of surface-active contaminants, which tend to accumulate at the interface. Frumkin and Levich (1947) gave the most accepted mechanism for mobility hindrance. Surfactant adsorbed on the bubble surface is convected from the front to the bubble's trailing end. The nonuniformity of surfactant distribution on the surface induces a tangential gradient of surface tension, which in turn causes a tangential stress opposing the flow shear stress (Scriven, 1960). This so-called Marangoni effect retards surface motion and increases the drag coefficient.

An important factor determining bubble mobility is size. Different behavior of "small" and "large" bubbles have been reported in the literature, and the critical size below which a gas bubble behaves as a rigid sphere has been discussed (Garner and Hammerton, 1954; Calderbank, 1959; Calderbank and Moo-Young, 1961; Kawase and Moo-Young, 1992).

Correspondence concerning this article should be addressed to J. M. T. Vasconcelos.

For example, "small" bubbles are particularly subject to retardation of rise velocity relative to the fluid sphere theoretical value. The reason for this is that contamination affects more significantly smaller bubbles. Concentration and surface-tension gradients are more pronounced for "small" than for "large" bubbles, the surface of which is little affected by impurities and moves freely (Clift et al., 1978). It has therefore been argued that bubbles and drops, however small, will have a mobile interface, so long as they are free from surfactants, and this has been experimentally verified with drag coefficients (Duineveld, 1995). Differences in mass transfer may still be explained by the fact that smaller bubbles tend to spend a longer time in the experimental apparatuses, due to lower rise velocity, and are thus subject to larger contamination periods.

Bubble mobility, hydrodynamic characteristics, and mass transfer have been shown by Raymond and Zieminski (1971) to be functionally related. These authors showed that an interdependence exists between the drag coefficient and the mass-transfer coefficient, independently of bubble size, surfactant type, and concentration. Koide et al. (1974) and Takemura and Yabe (1999) later reported similar relationships. The decrease of the mass-transfer coefficient due to surfactants has been clearly shown to be of a hydrodynamic rather than of a surface-resistance nature (Raymond and Zieminski, 1971).

The film mass-transfer coefficient for the mobile surface, as predicted using Eq. 1, is about three to five times greater than for the immobile surface, for typical situations of bubbles in water. Predictions according to Eq. 1 match approximately mass-transfer data for "large" bubbles (> 2.5 mm diameter), including those of the spherical-cap type (Calderbank and Lochiel, 1964; Calderbank, 1967; Zieminski and Raymond, 1968; Calderbank et al., 1970). Equation 2 has been verified with very small bubbles (< 0.15 mm diameter) by Motarjemi and Jameson (1978), or even with just so-called "small" bubbles (< 2.5 mm diameter) by Calderbank (1959), Calderbank and Moo-Young (1961), and Brankovic et al. (1984). Experimental film coefficients from the literature tend to fall within the limits imposed by Eqs. 1 and 2, depending on water purity and bubble size. This is verified both in works on bubble swarms (Kawase and Moo-Young, 1992), as well as in single-bubble studies (Deindoerfer and Humphrey, 1961; Koide et al., 1976; Hills et al., 1982; Schulze and Schlünder, 1985a,b; Bischof et al., 1991; Takemura and Yabe, 1999). It is also usual to find a large scatter of results in ordinary water. This is attributed to time effects in poorly reproducible processes, like bubble formation and detachment, where surfactants are inevitably present (Baird and Davidson, 1962; Zieminski and Raymond, 1968).

If a bubble of relatively constant diameter is introduced in a liquid medium with a finite concentration of surface-active contaminant, its mass-transfer coefficient should decrease with time, as surfactant is adsorbed from the liquid bulk. The effect of age on bubbles of fixed size is indeed known to reduce k_L from values given by Eq. 1 toward values given by Eq. 2, and is most noticeable at small bubble diameters (Calderbank and Lochiel, 1964). Decrease of k_L with time was found for bubbles in free rise (Baird and Davidson, 1962; Leonard and Houghton, 1963; Bischof et al., 1991), using either photography (Deindoerfer and Humphrey, 1961), or the constant-volume technique (Koide et al., 1974), or LDA (Brankovic et al., 1984). An identical result was found in a special case where bubble size was kept unchanged by feeding gas to it through a capillary (Griffith, 1960). The same phenomenon has sometimes been attributed to "end effects" in the experimental columns, because k_L decreases with increasing height (Deindoerfer and Humphrey, 1961; Hills et al., 1982).

A different kind of experiment was set up by Schulze and Schlünder (1985a), who stabilized a bubble in a liquid flow in essentially the same way as Ledig and Weaver (1924). They used a conical glass tube to capture bubbles against a descending water stream. This allowed them to visually follow a bubble for a longer time, as it simultaneously dissolved and gathered contaminant. They systematically found, for highly soluble gases, an initial period with a constant large mass-transfer coefficient, followed by a regime of constant much lower mass-transfer coefficient, consistent with Eq. 2. These results were only later interpreted by Davies (1986) in terms of surface contamination. For slowly dissolving gases, like O_2, N_2, H_2, Ne, and He, the first regime could not be observed by Schulze and Schlünder (1985a) for two reasons: (1) change in bubble dimensions is hardly detectable in the time span available, of the order of seconds, and (2) the effect of surfactants is still stronger when the gas solubility decreases (Liao and McLaughlin, 2000). Schulze and Schlünder's results also suggest that the transition from mobile to immobile interface may be abrupt, that is, that there is a critical surface concentration of surfactant above which surface mobility abruptly ends.

In the present work, a similar technique is used with the possibility of water decontamination, to investigate mass transfer both in clean and contaminated bubbles of low-solubility gases, and to study the transition between these situations. A model for the accumulation of impurities at the bubble interface is proposed, based on the "stagnant cap model" (Griffith, 1962; Davis and Acrivos, 1966; Sadhal and Johnson, 1983; Cuenot et al., 1997; Ponoth and McLaughlin, 2000).

Modeling

Bubble shape and geometry

Gas bubbles are nonspherical, except when interfacial tension and viscous forces are much more important than inertial forces (Clift et al., 1978). Generalized correlations have been given in the literature to predict bubble shape in motion through liquids (Grace et al., 1976). Bubbles in water in the $2 < d_e < 18$-mm size range are ellipsoidal in shape (Calderbank and Lochiel, 1964), but flattening of the spherical shape has no important influence on the mass-transfer coefficient (Lochiel and Calderbank, 1964). The characteristic bubble dimension is the diameter of the volume-equivalent sphere, d_e, calculated from the major and minor axes in two-dimensional projection, a and b, respectively

$$d_e = (a^2 b)^{1/3} \tag{3}$$

The surface area of ellipsoidal bubbles is higher than that of spherical bubbles of the same volume. The difference depends only on the aspect ratio a/b. For aspect ratio 1.5, the

error is only 3%, but, for the maximum observed aspect ratio in this work ($a/b \sim 3$), it is more than 25%. In the separate supplement to this article, a method is given to calculate the ellipsoidal surface area, A, from the equivalent diameter, d_e, based on a shape factor f, according to

$$A = f\pi d_e^2 \tag{4}$$

where f is a function of a/b. The aspect ratio a/b correlates linearly with d_e, so that

$$\frac{a}{b} = c_1 d_e + c_0 \tag{5}$$

where coefficients c_0 and c_1 are obtained from experimental data.

Bubble dissolution model

The dissolution of a pure gas bubble in unsaturated liquid is described by the equation that defines the liquid side mass transfer coefficient, k_L

$$-\frac{dn}{dt} = k_L A(C^* - C), \tag{6}$$

where n is the number of gas mols, A is the bubble surface area, C^* is the saturation concentration, and C is the bulk concentration of dissolved gas. Combining Eq. 6 with the ideal gas law, we find after integration at constant pressure that the diameter of spherical bubbles decreases linearly with time at a rate proportional to k_L.

When the gas in the bubble has more than one component or when it is impossible to completely free the liquid from other gaseous solutes that can undergo counterdiffusion, a balance such as Eq. 6 must be set up for each gaseous solute. For air, in particular, three components are considered—nitrogen, oxygen, and argon—which form 99.97% of its molar composition. Since these components are gases of low solubility in water, the gas-side resistance can be neglected and the mass-transfer rate equations for each component are analogous to Eq. 6

$$\frac{dn_i}{dt} = -k_{Li} A(C_i^* - C_i) \qquad (i = N, O, A) \tag{7}$$

where the subscripts refer to component i (N = nitrogen, O = oxygen and A = argon). After several assumptions are made, Eq. 7 becomes (see the separate supplement)

$$\frac{dn_i}{dt} = -k_L M_i F(n_N + n_O + n_A)\left(\frac{n_i}{n_N + n_O + n_A} - Y_i\right) \qquad (i = N, O, A) \tag{8}$$

where k_L is the liquid-side mass-transfer coefficient referred to oxygen diffusion in water, M_i and Y_i are constants, and $F(n_N + n_O + n_A)$ is a function of the total number of mols.

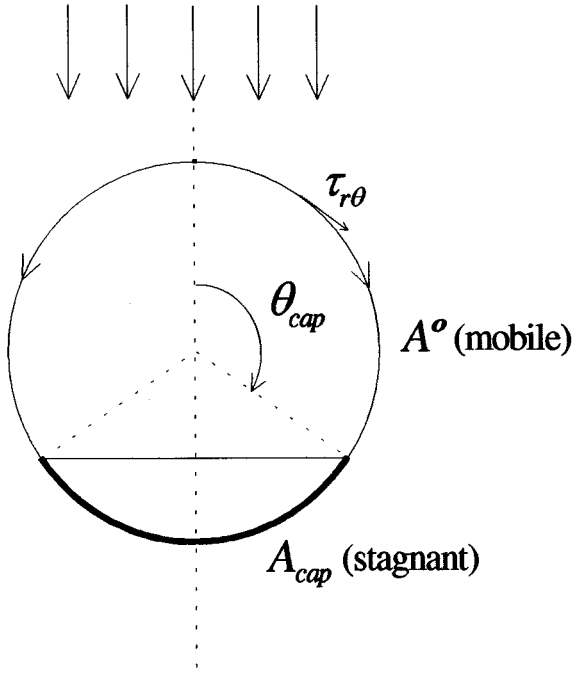

Figure 1. Stagnant cap model.

Equations 8 form a system of three first-order differential equations in $n_N(t)$, $n_O(t)$, and $n_A(t)$ with k_L as a parameter. Numerical calculation of the number of mols leads to computation of the bubble volume, and thus $d_e(t)$. Fitting of computed $d_e(t)$ to experimental measurements allows the k_L value to be found.

Surfactant accumulation model

The model follows the stagnant-cap model assumption that adsorbed surfactant molecules are dragged toward the rear of the bubble by adjacent liquid (Griffith, 1962). If surface convection is fast compared to both bulk diffusion and both adsorption and desorption, the adsorbed surfactant is collected in a stagnant-cap region, leaving the frontal region virtually uncontaminated and thus freely mobile (Cuenot et al., 1997).

Although mass transfer of surfactants is difficult to describe, it is assumed that diffusion controls the surfactant transport from the bulk, as if it were insoluble (Sadhal and Johnson, 1983; Ponoth and McLaughlin, 2000). Stagnant-cap size is a function of the bulk concentration of surfactant and, if the bubble is small enough, the cap may cover the entire surface (Davis and Acrivos, 1966).

The rate of diffusion of surfactant from the bulk to the surface is described in terms of a mass-transfer coefficient, k_S. The accumulation rate of surfactant on the stagnant cap also depends on the surfactant concentration in the bulk, C_∞, and on the available clean surface area, A^o (see Figure 1). Since the latter is the total surface area, A, minus the cap surface area, A_{cap}, the following equation can be written

$$\frac{dn_S}{dt} = k_S(A - A_{\text{cap}})C_\infty \tag{9}$$

where n_S is the number of surfactant mols in the stagnant cap.

If a_S is the area occupied by a mol of surfactant, then Eq. 9 becomes ($A_{\text{cap}} = n_S \cdot a_S$)

$$\frac{dA_{cap}}{dt} = k_S a_S (A - A_{\text{cap}}) C_\infty \tag{10}$$

Since we are considering mass transfer to a mobile surface, the mass-transfer coefficient, k_S, must obey Higbie's relationship with bubble diameter, d_e:

$$k_S = k' d_e^{-1/2} \tag{11}$$

Hence

$$\frac{dA_{\text{cap}}}{dt} = k' a_S C_\infty d_e^{-1/2} (A - A_{\text{cap}}) \tag{12}$$

where factor k', molar area a_S, and bulk concentration C_∞ can be lumped into one single parameter, k:

$$k = k' a_S C_\infty \tag{13}$$

The resulting equation for the growth of the contaminated surface with time is the following:

$$\frac{dA_{\text{cap}}}{dt} = k d_e^{-1/2} (A - A_{\text{cap}}) \tag{14}$$

Equation 14 describes surface aging, from the initial clean condition ($A_{\text{cap}} = 0$) when the bubble interface is fully mobile, up to a critical condition at diameter d_e^*, where interfacial movement becomes hindered and the bubble begins to behave like a solid sphere. It must be noted that parameter k (Eq. 13) is probably not constant, because compression of surfactant molecules along the growth of the stagnant cap is progressive (see Liao and McLaughlin, 2000). We assume, however, that the molar area, a_S (Eq. 10), hence k, take constant values for all bubbles at immobilization. In Eq. 14 $A(t)$ is calculated from $d_e(t)$, according to the method outlined in the section on bubble shape and geometry.

The time-dependent cap angle $\theta_{\text{cap}}(t)$ is geometrically related with the clean surface area A^o at time t; thus, with actual $A(t)$ and $A_{\text{cap}}(t)$ (see Figure 1)

$$\theta_{\text{cap}} = \cos^{-1}\left[1 - \frac{2}{\pi d_e^2} \cdot (A - A_{\text{cap}})\right] \tag{15}$$

The criterion to find the cap angle θ_{cap}^* that immobilizes the interface is closely related to the hypothesis of Frumkin and Levich (1947). According to it, the hindering action is described by the force balance on the surface between the surface-tension gradient and the viscous shear stress $\tau_{r\theta}$ (Griffith, 1962)

$$\frac{1}{r} \cdot \frac{d\sigma}{d\theta} + \tau_{r\theta} = 0 \tag{16}$$

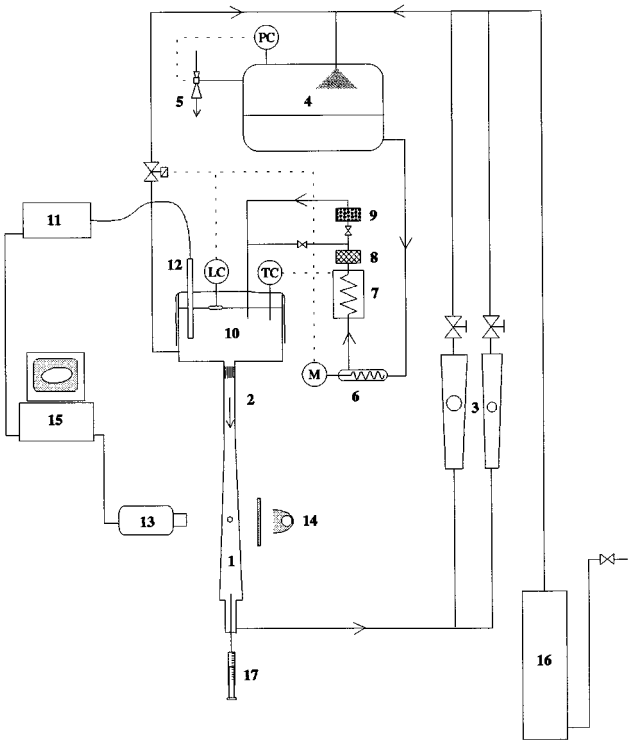

Figure 2. Experimental setup.

where r is the bubble radius and $\tau_{r\theta}$ is a function of d_e and of bubble rise velocity v_t (Bird et al., 1960). Integration of Eq. 16 between 0 and θ_{cap}^*, at immobilization, assumes that a constant difference ($\sigma_{\max} - \sigma_{\min}$) is reached between the surface tension at the front stagnation point and its value on the cap, for all bubbles. The following condition is thus found at the transition point in the intermediate flow regime ($Re < 500$), where $v_t \approx$ constant $\times\, d_e$ (Clift et al., 1978)

$$d_e^* \cdot (1 - \cos\theta_{\text{cap}}^*) = K \tag{17}$$

where K is a characteristic constant for each surfactant, which depends on the surface pressure at immobilization ($\sigma_{\max} - \sigma_{\min}$), shown by Davis and Acrivos (1966) to determine the relative size of the cap. $K/2$ represents the height of the spherical segment defined by the top clean interface when the bubble is immobilized.

Equation 14 can be integrated from time zero to $t = t^*$, where the angle θ_{cap} given by Eq. 15 reaches a value θ_{cap}^* that satisfies the critical condition stated by Eq. 17. k in Eq. 14 and K in Eq. 17 are treated as optimization parameters, by fitting the model output to experimental $d_e(t)$ data.

Experimental

The experiments were performed on free-floating bubbles that were held stationary by means of a downward liquid flow. The experimental set-up is shown in Figure 2.

Water flowed downward in the observation section (1) consisting of a divergent square channel 500 mm high, with the cross section increasing from 10×10 mm^2 to 40×40 mm^2.

An angle of divergence of nearly 1.7° was thus established in the channel, well below the lower limit of 7–8° for boundary-layer separation (Komori et al., 1985). Upstream of the observation section, a flow distribution and calming section (2) was provided, consisting of a honeycomb and a stainless-steel screen of 48 mesh, followed by a 200-mm square tube of $10\times$ 10-mm^2 cross section. After passing through a flow measurement section (3), consisting of two calibrated rotameters fitted with outlet valves, water was circulated in closed circuit. Water was first sprayed and degassed by vacuum stripping of dissolved air in a thick glass vessel of 25×10^{-3}-m^3 capacity (4) provided with a pressure controller and a water jet pump (5). A screw pump driven by a variable-speed motor (6) pumped the liquid from the degasser. After being cooled to 20°C in a heat exchanger (7), water passed through a 1-μm particle-retention filter (8), and, optionally, an activated-carbon filter for adsorption of organic materials (9). Water was finally fed into an open-air overhead tank (10), covered with plastic film for dust-particle elimination. A level controller was mounted in the overhead tank, to keep hydrostatic pressure constant. Water saturation with air was monitored using two WTW Ox340 oxygen meters with resolution 0.1% (11), equipped with CellOx325 galvanic probes (12). Distilled water was fed to the system. Water treated through the activated-carbon filter (9) will be referred to as "clean" water. Alternatively, untreated water from an ion exchanger (16) was used for comparison purposes.

Introducing gas with a needle and a calibrated syringe (17) produced bubbles of equivalent diameter 1 to 9 mm, approximately. The gases used were air, nitrogen, oxygen, argon, and ethylene. Bubble position was stabilized by liquid velocity gradient and adjusted by liquid flow rate. Pressure in the degassing vessel was set in the 4×10^3 to 8×10^4-Pa range to impose the water unsaturation and thus the concentration driving force. The average bubble slip velocity v_t was computed from the liquid flow rate and free cross-sectional area.

The bubble size was measured using a video technique to obtain projected bubble images. Images were recorded using a COHU 2152 RS-170 monochrome video camera (13) with standard framing rate 50 s^{-1}, resolution 560×450, manual gain, and electronic shutter speed at 1000 s^{-1}. The camera was fitted with an objective adapter $0.5\times$ and mounted on a low magnification LEICA MS5 microscope equipped with an Achromat $0.32\times$ objective of 297-mm focal length. Magnification ratios of 12.8, 20, and 32 times actual size were obtained in a 17-in. PC monitor using the magnification changers $1.6\times$, $2.5\times$ and $4\times$, respectively. Diffuse backlighting was provided by means of a 40-W lamp and a diffuser (14) at a distance of nearly 10 cm. The images were received in a 14-in. TV monitor and digitized into 720×576 pixels with a data-acquisition board Tekram C210 installed in a PC (15). Image analysis and measurement were performed using ZEISS imaging software KS100. The installed digital capability allowed the two adjacent frames of the standard video system to be separated. Frames are generated every 1/25 s, but they correspond to bubble snapshots captured in 1/1000 s, a short enough time interval for the bubble not to move significantly. Estimation of bubble displacement is about 2% of its diameter, based on an oscillation amplitude of a half diameter for 5–6-mm bubbles (Montes et al., 1999), and rocking frequency 10 Hz calculated for maximum Strouhal number 0.3 (Lindt and de Groot, 1974). The resolution was 34, 20, and 13 μm per pixel, depending on the magnification. The error in bubble axis measurement based on 2 pixel inaccuracy is lower than 3%, for bubble diameter down to 0.9 mm.

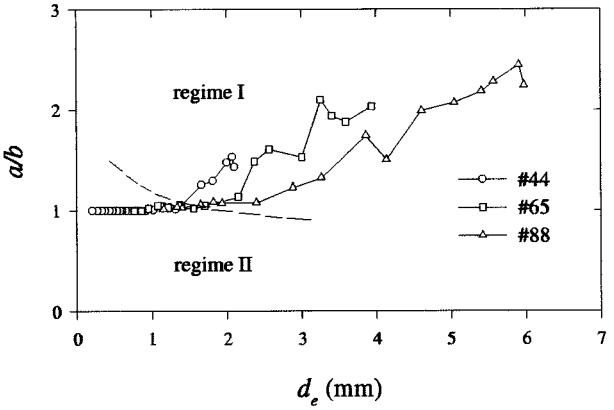

Figure 3. Examples of variation of bubble aspect ratio a/b with equivalent diameter d_e.

Results and Discussion

Bubble shape

Figure 3 shows the variation of the bubble aspect ratio a/b with d_e, for three examples of air-bubble absorption in "clean" water starting with different initial diameters.

Two regimes are apparent from Figure 3. In the initial regime (regime I), the bubble surface is extremely mobile and deformable, while being randomly submitted to oscillations. In this regime, the bubble shape is far from spherical, especially for larger bubbles (4–8 mm), as illustrated by a/b values in the figure. Yet, after a transition diameter is reached and the bubble shape approaches spherical, the oscillations suddenly become dampened and the bubble stabilizes as it slowly shrinks. In this final regime (regime II), the variation of a/b with d_e is smooth and nearly the same for all bubbles (in Eq. 5, $c_1 = 0.64\times10^2$ m^{-1} and $c_0 = 0.951$). In regime I, not only does a/b vary strongly with d_e (averaged c_1 in Eq. 5 is 0.337×10^3 m^{-1}), its exact value may only be predicted if the "history" of the bubble is known. Coefficient c_0 in Eq. 5, for regime I, may be given as a function of d_e^* (m) by the following relationship

$$c_0 = -0.273\times10^3 d_e^* + 0.951 \qquad \text{(regime I)} \qquad (18)$$

Bubble dissolution

Figure 4 presents how the diameter of a dissolving air bubble changes with time in two different liquid media under the same experimental conditions. Experiment #22u was carried out in untreated water at 74.5% air saturation and 20.2°C. As shown in Figure 4, the dissolution has taken place in this case at a constant rate. Experiment #75 was performed at approximately the same dissolved air saturation (74.4%) and temperature (20.0°C), but in so-called "clean" water. A fast initial regime is observed in this experiment, followed by the regime of a much lower absorption rate that is suddenly similar to that of experiment #22u.

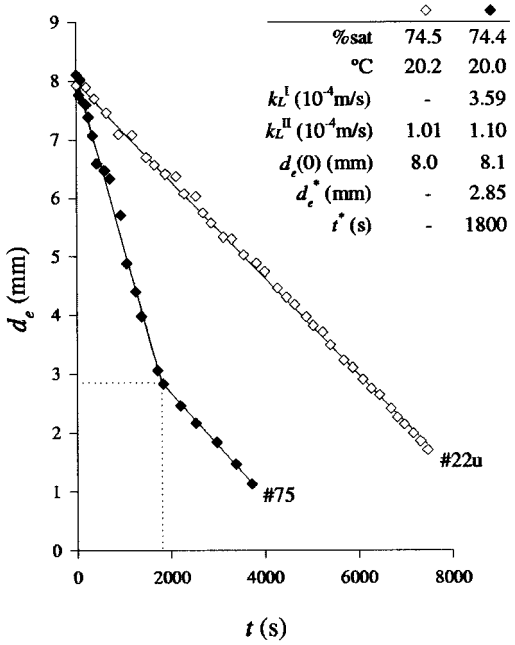

Figure 4. Air bubble dissolution in untreated (#22u) and "clean" water (#75).

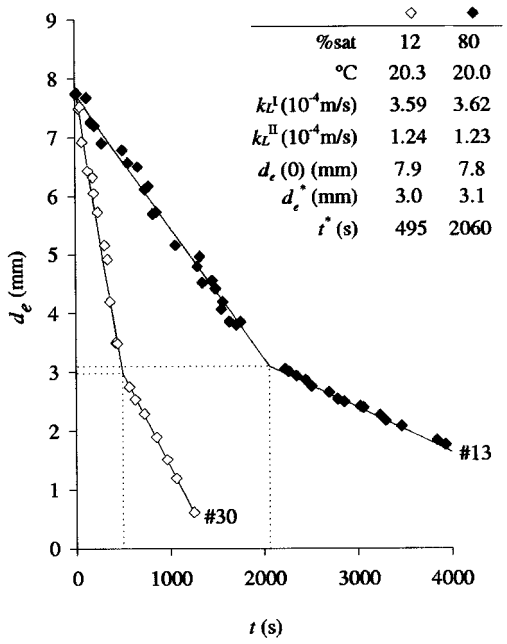

Figure 5. Effect of dissolved-air concentration.

These findings are compatible with the data by Schulze and Schlünder (1985a). In the case of untreated water, essentially the same result was obtained as was found by them with low-solubility gases. In "clean" water, two absorption regimes are clearly distinguished, but in their work this was only possible with highly soluble, and therefore, quickly dissolving gases. Furthermore, the time span of the initial absorption regime is here orders of magnitude greater than in their case. The concentration of impurities in water is thus seen to be critical for the detection of two absorption regimes, since in a relatively "dirty" system, as in Schulze and Schlüder's setup or in experiment #22u, the enhanced absorption period is too short to be detectable with slowly dissolving gases.

Experimental data from Figure 4 show that the d_e variation with time is very approximately linear in both regimes, as happens with a pure gas bubble, where the slope is proportional to k_L (see the section on the bubble dissolution model). This was systematically observed with air bubbles, although not in general with other gases. Air bubbles were therefore particularly useful for the detection of an abrupt transition between the fast and the slow mass-transfer regimes, since the slope could be assumed to be roughly proportional to k_L. The transition agreed approximately with the transition of the bubble-shape regimes previously mentioned. The average values of the mass-transfer coefficient in the initial and final regimes, k_L^{I} and k_L^{II}, respectively, were determined for all gases by applying the bubble dissolution model. In Figure 4, as well as in further cases, lines representing model simulations were superimposed on the experimental data for comparison. Simulation lines confirm that, for air bubbles, d_e varies linearly with time. The mass transfer coefficient in the fast absorption regime of experiment #75 was $k_L^{\mathrm{I}} = 3.59 \times 10^{-4}\,\mathrm{m \cdot s^{-1}}$, while in the slow absorption regime $k_L^{\mathrm{II}} = 1.10 \times 10^{-4}\,\mathrm{m \cdot s^{-1}}$ was comparable with the single k_L value of $1.01 \times 10^{-4}\,\mathrm{m \cdot s^{-1}}$ in experiment #22u.

The effect of dissolved-gas concentration is shown in Figure 5. The graphs in this figure register the dissolution history of two air bubbles of approximately the same initial size in "clean" water at 12% and 80% saturation. Although the dissolution is about four times faster in the first case, the calculated values of either k_L^{I} or k_L^{II} are very similar in both liquids. The only detectable effect of water saturation on the mass-transfer rate is thus through the driving force. It is interesting to note that the transition diameter is about the same in either case (~ 3 mm), despite the fact that the transition time differs by more than 300%. Simulation lines show good agreement between model and experiments.

The initial bubble size affects the results, as illustrated in the examples presented in Figure 6. Three different air bubbles are shown dissolving into the same water at $\sim 50\%$ air saturation. Data points and model lines attest model conformity with experiments. Transition time is again different from case to case, but now the same is true for the transition diameter as well. As far as the accuracy of the results allows us to assess, the transition diameter, d_e^*, seems to depend only on the initial diameter, $d_e(0)$. Figure 7 uses additional data from other experiments to illustrate an apparent correlation between d_e^* and $d_e(0)$. As for the transition time, t^*, besides its dependence on water saturation, as seen earlier, it also depends on the initial diameter. Figure 8 collects data that clearly support this conclusion.

Analysis of Figure 6 still reveals that the slope, and therefore the mass-transfer coefficient increases as $d_e(0)$ decreases, particularly in regime I. This is shown more clearly in Figure 9, where k_L^{I} and k_L^{II} are represented as a function of the averaged value of d_e in each period. The variation of k_L^{I} with average d_e is shown in Figure 9 to be very pronounced, when compared to k_L^{II}. The increase of k_L^{I} with decreasing bubble size is consistent with Higbie's equation for mobile interface (Eq. 1), as demonstrated by its represen-

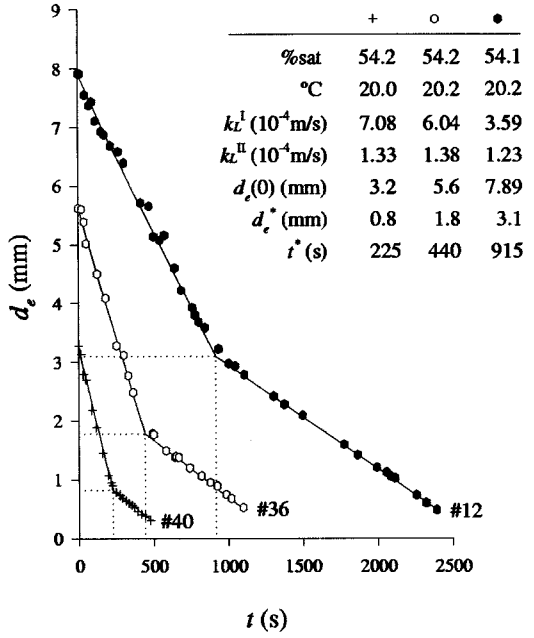

Figure 6. Effect of initial bubble size.

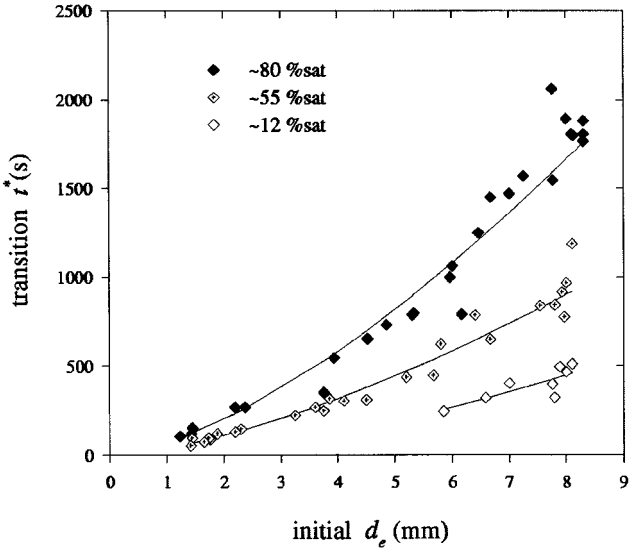

Figure 8. Correlation of transition time t^* with dissolved gas concentration and initial diameter of air bubbles.

tative line in Figure 9. Calculated k_L^I data are comparable with results by Zieminski and Raymond for CO_2 (Zieminski and Raymond, 1968; Raymond and Zieminski, 1971). Analogously, the k_L^{II} data are consistent with Froessling's equation for rigid spheres (Eq. 2), also shown in the same figure.

The dissolution of bubbles of different composition is presented in Figure 10. Nitrogen bubbles are not expected to behave very differently from air bubbles, as is shown in Figure 10a, except for an initial time interval, where linearity is delayed by oxygen counterdiffusion. Although they have similar diffusivity and solubility in water (see gas properties in the separate supplement), oxygen and argon bubbles are shown in Figures 10b and 10c to dissolve differently. This is because the air components, namely nitrogen and oxygen, are dissolved in the water. In either case, as the initial bubble gas dissolves and diffuses into the liquid, the counterdiffusion of nitrogen into the bubble volume opposes bubble contraction. In the argon-bubble case, this effect is reinforced by additional counterdiffusion of oxygen. Bubbles made of ethylene, which is more soluble and less diffusive than any of the air

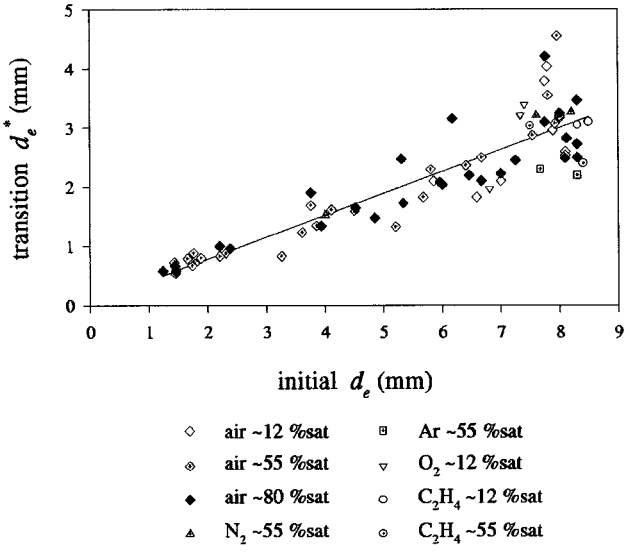

Figure 7. Correlation of transition diameter d_e^* with initial diameter.

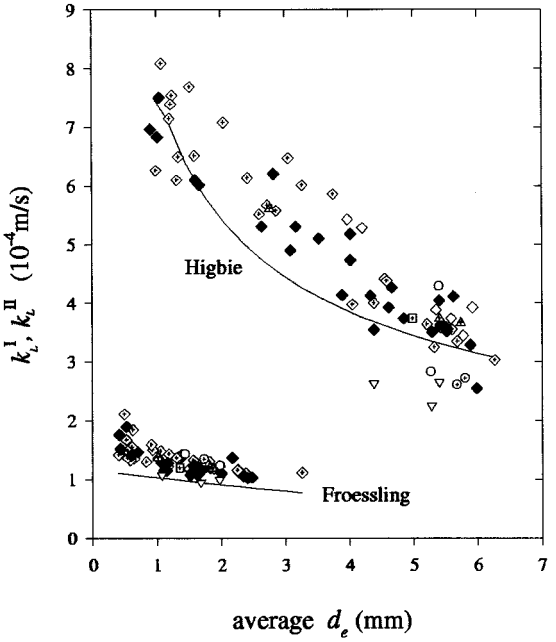

Figure 9. Mass-transfer coefficient k_L vs. average d_e in regimes I and II (same legend as Figure 7).

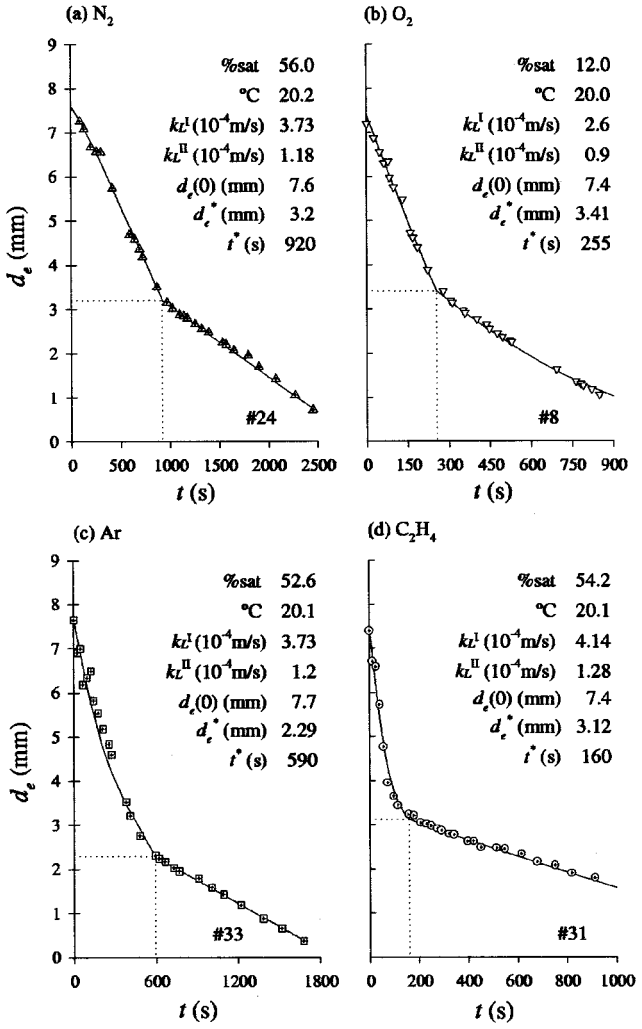

Figure 10. Dissolution of bubbles of different composition.

components (see separate supplement), clearly show that d_e diminution is slowed down by the counterdiffusion of nitrogen and oxygen from the liquid (Figure 10d). In the examples of Figure 10, curved lines are the general case. In any event, good agreement is found in these graphs between the experiments and the bubble-dissolution model. The ethylene case was simulated using a four-component version of the model.

From all the bubble-dissolution experiments that were carried out under different conditions in "clean" water, neither constant time nor constant diameter values were found to characterize the transition from the regime of a fast to that of a slower mass-transfer rate. We propose to interpret the experimental results in the light of the surfactant accumulation model.

Surfactant effects

According to our simplified version of the stagnant-cap model, the sudden change in the mass-transfer rate corresponds to the blocking of the interface after enough contaminant material has been collected at the bubble surface. The immobilization of the interface is considered to occur at the moment when the clean surface at the front of the bubble is reduced to a critical extent. This is as much the result of surfactant accumulation at the rear end as of simultaneous bubble shrinking. It is thus evident that neither d_e^* nor t^* should be constant in the various experiments. As predicted from Eq. 17, the criterion of mobile-to-rigid transition is determined instead by a fixed value of K, which represents twice the height of the clean spherical segment at the top. If this interpretation is valid, then a constant K value must be found when different absorption experiments in the same liquid medium are put together.

The following range of experimental conditions was used: (1) $\sim$12, 50–55 and 75–80% saturation of dissolved air; (2) 1.1–8.5-mm initial bubble size; and (3) air, N_2, O_2, Ar, and C_2H_4 as the initial gas. Using data from 64 experiments, a two-parameter optimization of the surfactant-accumulation model was obtained. By minimizing the sum of squares of the relative errors in t^* to a value of 1.296, optimized parameters $k = 2.4\times10^{-5}$ m$^{1/2}\cdot$s^{-1} (Eq. 13) and $K = 1.2\times10^{-3}$ m (Eq. 17) were found.

The optimized k value may be compared with its estimate from Eq. 13 based on values of k', a_S, and C_∞ from the literature. We assume that the surfactant diffusivity in water, D_S, is O(10^{-9}) m$^2\cdot$s^{-1} (Davies, 1986), and that the bubble size is 1 to 5 mm, which corresponds to a rise velocity in contaminated water $v_t \sim 0.1$–0.2 m$\cdot$s^{-1}. Therefore, Higbie's mass-transfer coefficient, k_S, is related with the square root of bubble diameter by a factor $k' \sim 2\times10^{-5}$ m$^{3/2}\cdot$s^{-1} (Eq. 11). Considering that the typical molecular area of the close-packed monolayer films of long-chain compounds is around 5×10^{-19} m^2 (Lu et al., 2000), the area, a_S, occupied by a mol of surfactant is O(10^5) m$^2\cdot$mol^{-1}. Finally, since the bulk concentration of filtered impurities, C_∞, can be estimated as O(10^{-5}) mol$\cdot$m^{-3} (Davies, 1986), the order of magnitude of k predicted by Eq. 13 is O(10^{-5}) m$^{1/2}\cdot$s^{-1}. This compares favorably with the optimized value.

Concerning the optimized K, its value implies a transition cap angle, θ_{cap}^*, of 101° (Eq. 17) for a transition diameter of 1 mm ($Re \sim 100$). This is comparable with the $105° > \theta_{cap} > 95°$ range in which the drag of a contaminated bubble at $Re = 100$ is most sensitive to the cap angle (Cuenot et al., 1997). More importantly, it has been confirmed that a unique value of K satisfies all experimental data.

Figure 11 is a parity plot where calculated and measured values of transition time, t^*, are compared. Deviation is on average 11%, adding credibility to the surfactant accumulation model. As seen in Figure 11, deviations tend to become biased for t^* higher than 1000 s. The model underestimates the time needed for the surfactant to immobilize the interface of high residence time bubbles. This is the case of large-size bubbles subject to a low dissolution rate (high gas concentration in the water). One possible explanation is that the model does not take into account either surfactant desorption or, perhaps more significantly, the collapsing of the surfactant film, which is unable to support the long-standing shear of irregular character along the surface of the cap (Davis and Acrivos, 1966). In the case of slowly dissolving large bubbles, effective cap growing may thus be retarded relative to model prediction due to the loss of surface-active material from highly mobile and unevenly stressed interfaces.

A physical explanation can be offered for the sudden change from higher k_L^I to lower k_L^{II} at cap angle θ_{cap}^*. High

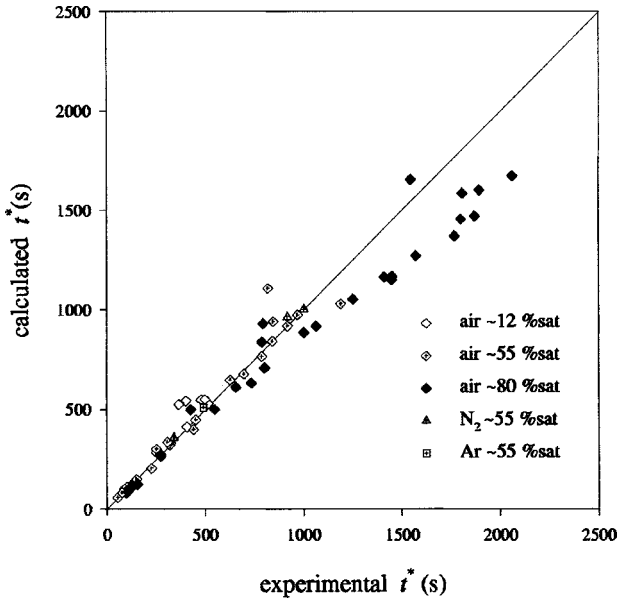

Figure 11. Calculated vs. experimental transition times.

k_L is related to interface movement, which implies forming a new surface by stretching. This requires energy, which is recovered in compression (Garner and Hammerton, 1954). Any loss of surface energy due to different interfacial tension between the bubble front and the leading edge of the cap, where the surface is compressed, must be compensated for by skin friction. If, however, the work done by the fluid is not enough, surface formation, and hence interface movement, stops. This can happen even if the front end of the bubble is clean, provided its extent is less than needed by a declining average value of the tangential stress component $\tau_{r\theta}$ along that surface (Figure 1).

Further work needs to be done to relate experimental data with the type, properties, and concentration of contaminant.

Conclusions

Two distinct mass-transfer regimes were clearly detected in the dissolution of single bubbles of low-solubility gases in liquid with very little contamination ("clean" water). The initial regime is characterized by fast absorption, with k_L in agreement with predictions from Higbie's theory for fully mobile interface. During the second regime, k_L is one-fifth to one-third of the initial value, now in accordance with that expected for rigid spheres. The transition between regimes is quite sharp, which allows definition of a transition time t^* and a transition diameter d_e^*. The transition values depend upon initial bubble size and mass-transfer driving force, spanning over 50 to 2,000 s and 0.5 to 4.5 mm, respectively. Both mass-transfer regimes had a counterpart in the bubble eccentricity regimes. In untreated water, only the rigid-bubble regime is identifiable.

Transition of mobile to rigid bubble was successfully interpreted and modeled in terms of the kinetics of the accumulation of surface-active material onto the bubble interface. The model includes two adjustable parameters, one that lumps unknown surfactant properties, the other a surface immobilization parameter. A single optimized value for each of these two parameters allows good estimation of transition time t^* (11% average deviation).

Acknowledgments

This work was supported by FCT—Fundação para a Ciência e a Tecnologia (Project Praxis/EQU/12066/98). The second author (S. P. O.) gratefully acknowledges financial support from FCT (Grant No. SFRH/BD/3229/2000).

Literature Cited

Baird, M. H. I., and J. F. Davidson, "Gas Absorption by Large Rising Bubbles," *Chem. Eng. Sci.*, **17**, 87 (1962).

Bird, R. B., W. E. Stewart, and E. N. Lightfoot, *Transport Phenomena*, Wiley, New York (1960).

Bischof, F., M. Sommerfeld, and F. Durst, "The Determination of Mass Transfer Rates from Individual Small Bubbles," *Chem. Eng. Sci.*, **46**, 3115 (1991).

Brankovic, A., I. G. Currie, and W. W. Martin, "Laser-Doppler Measurements of Bubble Dynamics," *Phys. Fluids*, **27**, 348 (1984).

Calderbank, P. H., "Physical Rate Processes in Industrial Fermentation, Part II.—Mass Transfer Coefficients in Gas-Liquid Contacting with and Without Mechanical Agitation," *Trans. Inst. Chem. Eng.*, **37**, 173 (1959).

Calderbank, P. H., "Gas Absorption from Bubbles," *Trans. Inst. Chem. Eng.*, **45**, CE209 (1967).

Calderbank, P. H., and M. B. Moo-Young, "The Continuous Phase Heat and Mass-Transfer Properties of Dispersions," *Chem. Eng. Sci.*, **16**, 39 (1961).

Calderbank, P. H., and A. C. Lochiel, "Mass Transfer Coefficients, Velocities and Shapes of Carbon Dioxide Bubbles in Free Rise Through Distilled Water," *Chem. Eng. Sci.*, **19**, 485 (1964).

Calderbank, P. H., D. S. L. Johnson, and J. Loudon, "Mechanics and Mass Transfer of Single Bubbles in Free Rise Through Some Newtonian and Non-Newtonian Liquids," *Chem. Eng. Sci.*, **25**, 235 (1970).

Clift, R., J. R. Grace, and M. E. Weber, *Bubbles, Drops, and Particles*, Academic Press, London (1978).

Cuenot, B., J. Magnaudet, and B. Spennato, "The Effects of Slightly Soluble Surfactants on the Flow Around a Spherical Bubble," *J. Fluid Mech.*, **339**, 25 (1997).

Davies, J. T., "Rates of Gas Absorption from Single Gas Bubbles," *Chem. Eng. Sci.*, **41**, 1928 (1986).

Davis, R. E., and A. Acrivos, "The Influence of Surfactants on the Creeping Motion of Bubbles," *Chem. Eng. Sci.*, **21**, 681 (1966).

Deindoerfer, F. H., and A. E. Humphrey, "Mass Transfer from Individual Gas Bubbles," *Ind. Eng. Chem.*, **53**, 755 (1961).

Duineveld, P. C., "The Rise Velocity and Shape of Bubbles in Pure Water at High Reynolds Number," *J. Fluid Mech.*, **292**, 325 (1995).

Frumkin, A., and V. G. Levich, *Zh. Fiz. Khim.*, **21**, 1183 (1947) (cit. Clift et al., 1978).

Garner, F. H., and D. Hammerton, "Circulation Inside Gas Bubbles," *Chem. Eng. Sci.*, **3**, 1 (1954).

Grace, J. R., T. Wairegi, and T. H. Nguyen, "Shapes and Velocities of Single Drops and Bubbles Moving Freely Through Immiscible Liquids," *Trans. Inst. Chem. Eng.*, **54**, 167 (1976).

Griffith, R. M., "Mass Transfer from Drops and Bubbles," *Chem. Eng. Sci.*, **12**, 198 (1960).

Griffith, R. M., "The Effect of Surfactants on the Terminal Velocity of Drops and Bubbles," *Chem. Eng. Sci.*, **17**, 1057 (1962).

Hills, J. H., C. J. Abbott, and L. J. Westall, "A Simple Apparatus for the Measurement of Mass Transfer from Gas Bubbles to Liquids," *Trans. Inst. Chem. Eng.*, **60**, 369 (1982).

Kawase, F., and M. Moo-Young, "Correlations for Liquid-Phase Mass Transfer Coefficients in Bubble Column Reactors with Newtonian and Non-Newtonian Fluids," *Can. J. Chem. Eng.*, **70**, 48 (1992).

Koide, K., T. Hayashi, K. Sumino, and S. Iwamoto, "Mass Transfer from Single Bubbles in Aqueous Solutions of Surfactants," *Chem. Eng. Sci.*, **31**, 963 (1976).

Koide, K., Y. Orito, and Y. Hara, "Mass Transfer from Single Bubbles in Newtonian Liquids," *Chem. Eng. Sci.*, **29**, 417 (1974).

Komori, K., A. Iguchi, and R. Izumi, "Characteristics of Turbulent Flow in Divergent Channels of Rectangular Cross Section," *Int. Chem. Eng.*, **25**, 97 (1985).
Ledig, P. G., and E. R. Weaver, "A Method for Studying the Rapid Absorption of Gases by Liquids," *J. Amer. Chem. Soc.*, **46**, 650 (1924).
Leonard, J. H., and G. Houghton, "Mass Transfer and Velocity of Rise Phenomena for Single Bubbles," *Chem. Eng. Sci.*, **18**, 133 (1963).
Liao, Y., and J. B. McLaughlin, "Dissolution of a Freely Rising Bubble in Aqueous Surfactant Solutions," *Chem. Eng. Sci.*, **55**, 5831 (2000).
Lindt, J. T., and R. G. F. de Groot, "The Drag on a Single Bubble Accompanied by a Periodic Wake," *Chem. Eng. Sci.*, **29**, 957 (1974).
Lochiel, A. C., and P. H. Calderbank, "Mass Transfer in the Continuous Phase Around Axisymmetric Bodies of Revolution," *Chem. Eng. Sci.*, **19**, 471 (1964).
Lu, J. R., R. K. Thomas, and J. Penfold, "Surfactant Layers at the Air/Water Interface: Structure and Composition," *Advances in Colloid and Interface Science*, **84**, 143 (2000).
Montes, F. J., M. A. Galan, and R. L. Cerro, "Mass Transfer From Oscillating Bubbles in Bioreactors," *Chem. Eng. Sci.*, **54**, 3127 (1999).
Motarjemi, M., and G. J. Jameson, "Mass Transfer From Very Small Bubbles—The Optimum Bubble Size for Aeration," *Chem. Eng. Sci.*, **33**, 1415 (1978).
Ponoth, S. S., and J. B. McLaughlin, "Numerical Simulation of Mass Transfer for Bubbles in Water," *Chem. Eng. Sci.*, **55**, 1237 (2000).
Raymond, D. R., and S. A. Zieminski, "Mass Transfer and Drag Coefficients of Bubbles Rising in Dilute Aqueous Solutions," *AIChE J.*, **17**, 57 (1971).
Sadhal, S. S., and R. E. Johnson, "Stokes Flow Past Bubbles and Drops Partially Coated with Thin Films. Part 1. Stagnant Cap of Surfactant Film—Exact Solution," *J. Fluid Mech.*, **126**, 237 (1983).
Schulze, G., and E. U. Schlünder, "Physical Absorption of Single Gas Bubbles in Degassed and Preloaded Water," *Chem. Eng. Process.*, **19**, 27 (1985a).
Schulze, G., and E. U. Schlünder, "The Effect of Multicomponent Diffusion on the Mass Transfer During Absorption of Single Gas Bubbles," *Chem. Eng. Process.*, **19**, 257 (1985b).
Scriven, I. E., "Dynamics of a Fluid Interface," *Chem. Eng. Sci.*, **12**, 98 (1960).
Takemura, F., and A. Yabe, "Rising Speed and Dissolution Rate of a Carbon Dioxide Bubble in Slightly Contaminated Water," *J. Fluid Mech.*, **378**, 319 (1999).
Zieminski, S. A., and D. R. Raymond, "Experimental Study of the Behavior of Single Bubbles," *Chem. Eng. Sci.*, **23**, 17 (1968).

Manuscript received May 17, 2001, and revision received Nov. 12, 2001.

See NAPS document no. 05607 for 5 pages of supplementary material. This is not a multiarticle document. Order from NPAS c/o Microfiche Publications, 248 Hempstead Turnpike, West Hempstead, NY 11552. Remit in advance in U.S. funds only $18.50 for photocoples or $5.00 for microfiche. There is a $25.00 invoicing charge on all orders filled before payment. Outside the U.S. and Canada, add postage of $4.50 for the first 20 pages and $1.00 for each of 10 pages of material thereafter, or $5.00 for the first microfiche and $1.00 for each fiche thereafter.